Arterivirus PLP2 : an OTU deubiquitinase that counteracts Innate Immunity

Kasteren, P.B. van

Chapter 4

Deubiquitinase function of arterivirus papain-like protease 2 suppresses the innate immune response in infected host cells

Puck B. van Kasteren, Ben A. Bailey-Elkin[1], Terrence W. James[1], Dennis K. Ninaber, Corrine Beugeling, Mazdak Khajehpour, Eric J. Snijder, Brian L. Mark[2], and Marjolein Kikkert[2]

Proc Natl Acad Sci U S A (2013) **110:**E838-47

[1] Both authors contributed equally to this work.

[2] Both authors contributed equally to this work.

ABSTRACT

Protein ubiquitination regulates important innate immune responses. The discovery of viruses encoding deubiquitinating enzymes (DUBs) suggests they remove ubiquitin to evade ubiquitin-dependent antiviral responses; however, this has never been conclusively demonstrated in virus-infected cells. Arteriviruses are economically important positive-stranded RNA viruses that encode an ovarian tumor (OTU) domain DUB known as papain-like protease 2 (PLP2). This enzyme is essential for arterivirus replication by cleaving a site within the viral replicase polyproteins, and also removes ubiquitin from cellular proteins. To dissect this dual specificity, which relies on a single catalytic site, we determined the crystal structure of equine arteritis virus PLP2 in complex with ubiquitin (1.45 Å). PLP2 binds ubiquitin using a zinc finger that is uniquely integrated into an exceptionally compact OTU-domain fold that represents a new subclass of zinc-dependent OTU DUBs. Notably, the ubiquitin-binding surface is distant from the catalytic site, which allowed us to mutate this surface to significantly reduce DUB activity without affecting polyprotein cleavage. Viruses harboring such mutations exhibited wild-type replication kinetics, confirming that PLP2-mediated polyprotein cleavage was intact, but the loss of DUB activity strikingly enhanced innate immune signalling. Compared to wild-type virus infection, beta-interferon mRNA levels in equine cells infected with PLP2 mutants were increased by nearly an order of magnitude. Our findings not only establish PLP2 DUB activity as a critical factor in arteriviral innate immune evasion, the selective inactivation of DUB activity also opens new possibilities for developing improved live attenuated vaccines against arteriviruses and other viruses encoding similar dual-specificity proteases.

SIGNIFICANCE STATEMENT

Many viruses encode proteases that cleave both viral and host substrates. Arteriviruses encode such a dual-specificity protease (PLP2) that removes ubiquitin from cellular proteins involved in host immunity. Based on a 3D-structure of PLP2, we engineered the protease to have diminished deubiquitinating activity without affecting its activity towards its viral substrate. Viruses expressing such engineered proteases displayed a significantly weakened ability to evade host immune responses. This demonstrates a crucial role for PLP2 in arterivirus immune evasion and opens new possibilities for developing improved attenuated virus vaccines against economically important arteriviruses and other viruses encoding similar dual-specificity proteases.

INTRODUCTION

The synthesis and post-translational cleavage of polyproteins is a common genome expression strategy employed by positive-stranded (+) RNA viruses of eukaryotes. It is used to cope with the consequences of cytoplasmic replication and the limitations of the eukaryotic translation machinery, which essentially preclude the use of (nuclear) RNA splicing and polycistronic mRNAs, respectively (1). The critical cleavage of these viral polyproteins into their functional subunits is mediated by internal virus-encoded proteases (2-5), many of which have been found to also target cellular substrates in order to promote virus replication or subvert host antiviral responses. Well-known examples of such dual-specificity proteases are the poliovirus 2A and hepatitis C virus NS3/4A enzymes that, in addition to the viral polyprotein, target host cell proteins involved in translation and innate immune signalling, respectively (6-10).

Arteriviruses are +RNA viruses that, together with the corona- and roniviruses, belong to the order *Nidovirales* and include equine arteritis virus (EAV) and porcine reproductive and respiratory syndrome virus (PRRSV). EAV is the family prototype and can cause abortion in pregnant mares, pneumonia in neonatal foals, and influenza-like illness in adult horses (11). PRRSV ranks among the most important swine pathogens and infections are characterized by reproductive failure in sows and severe respiratory disease in young pigs (12). As in all nidoviruses, the synthesis and cleavage of the replicase polyproteins (pp1a and pp1ab) are critical first steps in arterivirus infection. They are encoded by the 5'-proximal three-quarters of the 13-16 kb arterivirus genome and are the precursors of the nonstructural proteins (nsps) required for genome replication and transcription. In the case of EAV, at least 13 nsps are produced when the replicase polyproteins are cleaved by three virus-encoded proteases (13, 14), one of which is a papain-like protease (PLP2) located in the N-terminal region of nsp2 (15, 16). This enzyme cleaves the nsp2|nsp3 junction in pp1a and pp1ab, an event that is essential for virus replication since an EAV PLP2 active site mutant was previously found to be nonviable (17). In addition to this critical role in viral polyprotein maturation, arterivirus PLP2 was proposed to contribute to the evasion of host innate immune responses by removing ubiquitin (Ub) from cellular targets (18). Ub is an 8-kDa protein moiety that can be covalently attached to lysine residues of target proteins in a number of structurally different configurations, either by monoubiquitination or through the formation of polyubiquitin chains (19, 20). The effects of ubiquitination can range from targeting substrates for proteasomal degradation to initiating signalling cascades and - importantly - they can be reversed by deubiquitinating enzymes (DUBs), which thus allow for negative regulation of Ub-activated processes (21-24). The latter include the innate immune signalling cascades triggered by invading RNA

viruses (25, 26), which ultimately lead to the transcription of genes encoding beta interferon (IFN-β) and other pro-inflammatory cytokines (27, 28).

Arterivirus PLP2 and a protease domain found in the unrelated nairovirus Crimean-Congo hemorrhagic fever virus (CCHFV), were first identified as potential members of the ovarian tumor domain-containing (OTU) superfamily of DUBs on the basis of comparative sequence analysis (29). Several laboratories, including our own, subsequently confirmed that arterivirus PLP2s indeed have DUB activity that may be employed to remove Ub from innate immune signalling factors to suppress the induction of an antiviral state (18, 30, 31). The potential benefits of this strategy are highlighted by the fact that proteases from virus groups as diverse as arteri-, corona-, nairo-, picorna-, hepadna-, and herpesviruses have all been implicated in DUB-based innate immune evasion (18, 32-37). Thus far, however, direct evidence linking DUB activity to the suppression of innate immune responses in virus-infected cells has not been reported for any of these proteases.

Since the DUB activity of arterivirus PLP2 depends on the same active site mediating the critical nsp2|nsp3 cleavage, it has not been possible to independently study the role of PLP2 in polyprotein processing and immune evasion in the context of virus infection. Here we present the crystal structure of EAV PLP2 in complex with Ub at 1.45 Å resolution. The complex reveals a distinctly compact conformation compared to other OTU superfamily members and the incorporation of a unique zinc finger within the OTU-fold. Given these features, arterivirus PLP2 represents a novel subclass of zinc-dependent OTU DUBs. Importantly, the PLP2 active site is distant from its Ub-binding surface, allowing for the introduction of mutations in this region that dramatically reduced DUB activity, yet did not affect nsp2|nsp3 cleavage. Compared to wild-type EAV, viruses carrying these mutations elicited a significantly enhanced innate immune response in primary equine cells, while displaying wild-type replication kinetics. Taken together, our results demonstrate that PLP2 DUB activity indeed mediates innate immune suppression during arterivirus infection. The ability to selectively inactivate the PLP2 DUB function may thus contribute to the engineering of improved live attenuated vaccines against arteriviruses and other virus families encoding proteases with similar dual specificities.

RESULTS

EAV PLP2 adopts a compact OTU-domain fold with a unique integral zinc finger. Previously, EAV PLP2 was identified and characterized by a combination of bioinfor-

matics analysis and site-directed mutagenesis, and two residues in particular were implicated in catalysis: Cys270 and His332 (16). Throughout this paper, amino acid numbers refer to the sequence of full-length EAV pp1a. The crystal structure of EAV PLP2 (residues 261-392; 13.6 kDa) was determined as a covalent complex with the mechanism-based inhibitor $Ub_{(1-75)}$–3–bromopropylamine (Ub–3Br) (38, 39). Since the conservation of multiple cysteine residues and their demonstrated importance for protease function suggested that PLP2 could bind zinc (16), the crystal structure of the complex was determined by a multi-wavelength anomalous dispersion (MAD) phasing experiment using X-ray diffraction data collected over the zinc absorption edge (**Table IV-S1**). The resulting electron density map revealed residues 261-387 of PLP2 bound to a complete Ub molecule and allowed a model of the complex to be built and refined (R_{work}= 0.16, R_{free}= 0.18) to 1.45 Å resolution (**Figures IV-1A and B**).

The protease adopts a compact, two-domain fold with a shallow Ub-binding surface that directs the C-terminus of the bound Ub molecule (the 'distal' Ub in a Ub dimer) towards a solvent exposed active site that indeed includes Cys270 and His332 (**Figures IV-1A and B**). Domain I of PLP2 (residues 267-307 and 365-387) consists of a three-helix bundle (α1, α2, α4) packed against a two-stranded antiparallel sheet (β2↑ β6↓). Domain II centers on a four-stranded β-sheet (β1↑ β5↓ β4↑ β3↑) and an α-helix (α3) that together pack against helices α1 and α2 of domain I. Domain II comprises the majority of the Ub-binding surface, which is stabilized by four cysteine residues (Cys 319, 349, 354, 356) that coordinate a zinc ion with tetrahedral geometry (**Figure IV-1C**). Their arrangement forms a C4 zinc finger that resembles a C-terminal type zinc necklace motif (40). A large insertion between positions C1 (Cys319) and C2 (Cys349), which includes His332, appears to extend the stabilizing effect of the zinc finger throughout much of domain II. A fifth cysteine (Cys344) is located near the zinc ion but does not coordinate with it, consistent with other zinc necklace motifs that have been described (40) and with previous findings showing that a Cys344 to alanine mutation had no effect on catalytic activity of PLP2 (16). Three of the cysteines (Cys 319, 349, and 354) are fully conserved in arteriviruses, and mutational analysis of these residues and Cys356 demonstrated zinc binding to be essential for catalytic activity (16). Given its distance from the active site however (~25 Å) (**Figure IV-1B**), the zinc finger appears to play a structural role as opposed to participating in catalysis. Expression of PLP2 in *E. coli* grown in the absence of zinc (M9 medium) yielded insoluble protein, supporting the idea that the zinc finger is structural and is likely required for correct folding of the protease.

Consistent with OTU DUBs and papain-like cysteine proteases in general, the PLP2 active site contains a catalytic cysteine nucleophile (Cys270) and histidine (His332) residue, along with an asparagine (Asn263) that hydrogen bonds with the imidazole ring of His332 (**Figure IV-1D**). As expected, the side chain of Cys270 is covalently

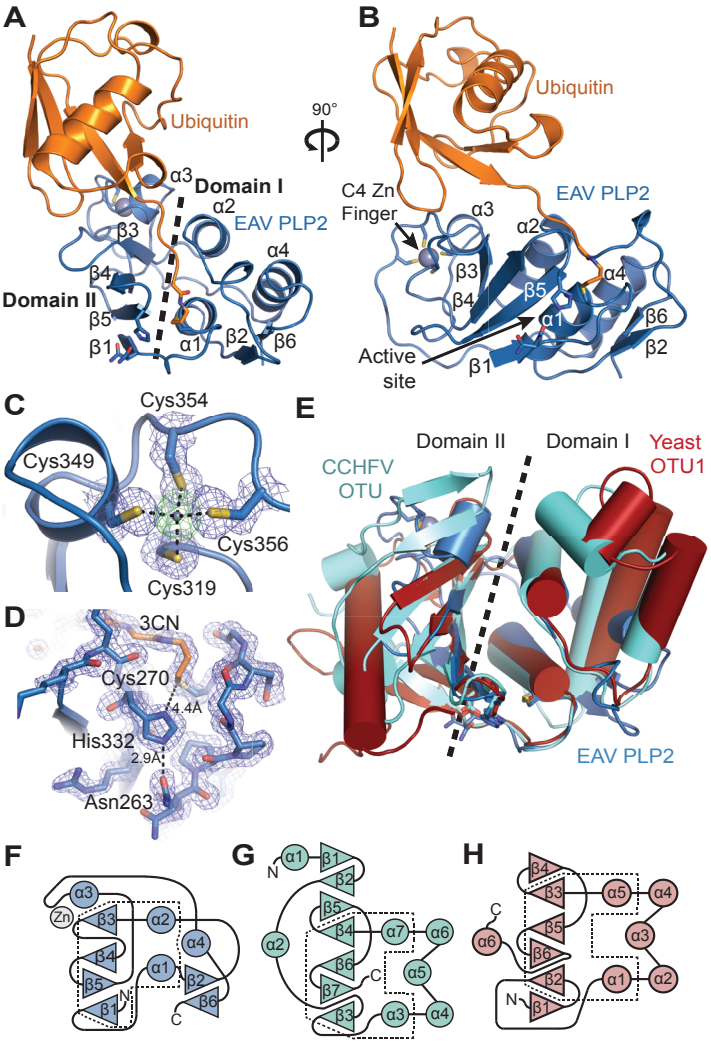

Figure IV-1: Structure of the EAV PLP2-Ub complex and superposition with yeast OTU1 and CCHFV OTU. A) Structure of EAV PLP2 (blue) bound to Ub (orange) showing the two-domain fold. **B)** 90 degree rotation of complex shown in *panel A*. **C)** Electron density for the C4 zinc finger motif. Blue density is a maximum-likelihood weighted $2F_o$-F_c map contoured at 1.0σ. Green density about the zinc atom (grey) is a F_o-F_c omit map contoured at 5.0σ. **D)** The catalytic triad of the EAV PLP2 active site. Blue density is a maximum-likelihood weighted $2F_o$-F_c map contoured at 1.0σ. The cysteine nucleophile (Cys270) is covalently linked to Ub via the 3NC linker, which replaces Gly76 of Ub. Asn263, which orients the imidazole ring of His332, occurs in two alternate conformations. **E)** Superposition of EAV PLP2 (blue), CCHFV OTU (cyan) and yeast OTU1 (red). PLP2 shares a conserved core of two central helices and a four-stranded beta sheet with CCHFV OTU and yeast OTU1. Topology diagrams for EAV PLP2, CCHFV OTU and yeast OTU1 are shown in panels **F, G, and H**, respectively. The region that is conserved amongst the enzymes is outlined (dashed box). Structural images were prepared using PyMOL (89).

coupled to the C-terminus of Ub via the 3-propylamine (3CN) modification, mimicking the acyl-enzyme intermediate step of the catalytic reaction and confirming the identity of Cys270 as the catalytic nucleophile.

Fold analysis of the PLP2 structure using the DALI server (41) revealed that its closest structural homologues indeed belong to the OTU superfamily of DUBs (29, 42). The most significant matches were to yeast Otu1 (38) (Z-score: 5.1) and the viral OTU protease from CCHFV (43-45) (Z-score: 4.6) (**Figure IV-1E**), followed by Otubain1 from human (46) and *Caenorhabditis elegans* (47) (Z-scores: 4.1 and 4.0, respectively), and the OTU-domain of human DUBA (48) (Z-score: 3.9). The sequence identity of the PLP2 regions that aligned with these OTU proteases was low (ranging from 9% for yeast Otu1 to 21% for human Otubain1); however, they accounted for ~60% of the total PLP2 structure and superposed well with the equivalent regions in the above proteins, with an average rmsd of ~2.8 Å. The greatest structural similarity between PLP2 and members of the OTU superfamily occurs at the active site and adjoining channel that binds the C-terminal RLRGG-tail of Ub.

The PLP2 zinc finger motif plays a central role in Ub binding. Arterivirus PLP2 and nairovirus OTU enzymes differ from eukaryotic OTU DUBs in that they also remove the Ub-like antiviral protein Interferon Stimulated Gene 15 (ISG15) from target proteins, a process also known as deISGylation (18, 49). ISG15 conjugation has been postulated to interfere with proper viral protein function, possibly through steric hindrance, although the exact mechanism underlying its antiviral activity is unknown (50). For CCHFV OTU, cross-reactivity with ISG15 arises primarily from a unique β-hairpin on the Ub-binding surface. The hairpin modifies the surface so that the viral enzyme binds the β-grasp folds of Ub and the C-terminal Ub-like domain of ISG15 in an orientation that is rotated nearly 75° with respect to that observed for Ub bound to a representative eukaryotic OTU DUB from yeast (Otu1) (43, 44). Surprisingly, the β-hairpin is absent in EAV PLP2 and replaced by helix α3 of the zinc finger motif (**Figure IV-2A**). However, in keeping with the role of the β-hairpin in CCHFV OTU, residues of helix α3 bind to the hydrophobic 'Ile44 patch' of Ub, a site commonly targeted by Ub-binding proteins (51), and they also assist in positioning Ub in a rotated manner equivalent to that observed for CCHFV OTU (**Figure IV-2B and C**).

Structure-guided decoupling of PLP2 deubiquitinase and polyprotein cleavage activities. Given the distance of helix α3 from the PLP2 active site (**Figure IV-1B**), we hypothesized that mutations could be introduced into this region of the Ub-binding surface that would selectively disrupt PLP2 DUB activity without affecting EAV polyprotein cleavage at the putative nsp2|nsp3 junction (RLIGG$^-$). While this sequence closely resembles the C-terminal tail of Ub (RLRGG$^-$), we postulated that the nsp2

sequence immediately upstream of the nsp2|nsp3 junction does not adopt a Ub-like fold and that the majority of the PLP2 Ub-binding surface is therefore not required for its cleavage. To test our hypothesis, we used the crystal structure to select three positions within the PLP2 Ub-binding surface (Thr312, Ile313, and Ile353), and engineered a panel of (combined) mutations (**Figures IV-2B and C**). Ile353 is located at the C-terminal end of helix α3 next to C3 (Cys354) of the zinc finger motif. It projects directly into the Ile44 patch of Ub where it makes extensive van der Waals interactions with Ile44, Val70, and Leu8. Given that Ile353 is located on the Ub-binding surface, we aimed to disrupt Ub binding by introducing various other residues at this position, including large bulky residues such as arginine and tryptophan. Thr312 and Ile313 are located closer to the active site, where they make additional hydrophobic interactions with Leu8, Leu71, and Leu73 of Ub. In an attempt to further disrupt the interaction between PLP2 and Ub, the mutations Thr312Ala and Ile313Val were also combined with changes at position Ile353. Given the close proximity of Ile313 to Leu73 of the RLRGG motif of Ub, mutation to valine was chosen to minimize adverse effects on nsp2|nsp3 cleavage.

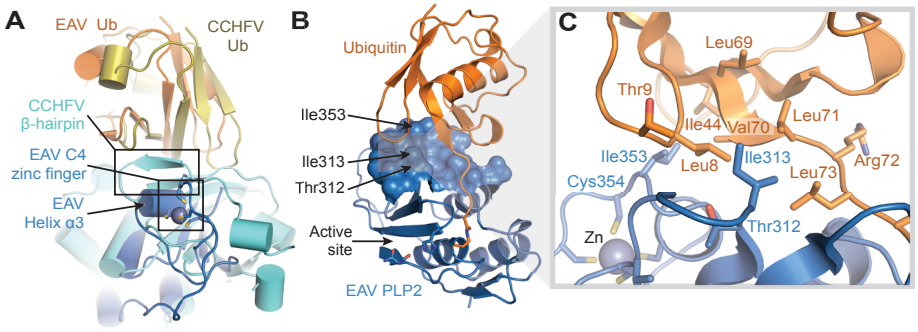

Figure IV-2: Ub-binding surface of EAV PLP2. A) Superposition of EAV PLP2 (blue) and CCHFV OTU (cyan) in complex with Ub. Both enzymes grasp Ub in a similar orientation, with the C4 zinc finger motif of EAV PLP2 replacing the β-hairpin of CCHFV OTU. **B)** EAV PLP2 (blue) bound to Ub (orange), showing the 612 Å^2 Ub-binding surface. Residues targeted for mutational analysis to disrupt DUB activity are indicated by arrows. **C)** Close-up of the EAV PLP2-Ub binding surface. EAV PLP2 residue Ile353 forms van der Waals interactions with Ile44, Leu8, and Val70 of Ub, whereas residues Thr312 and Ile313 interact with a hydrophobic patch on Ub (formed by residues Leu8, Val70, Leu71, and Ile73) closer to the active site of PLP2.

Before proceeding to infection experiments with mutant viruses, we used ectopic expression of PLP2 and an *in vitro* enzymatic assay to characterize the effect of various mutations at the positions described above on polyprotein processing and DUB activity. To this end, mutations were introduced into a mammalian expression vector

encoding a self-cleaving nsp2-3 polyprotein carrying an N-terminal HA-tag. Upon expression of nsp2-3 in HEK293T cells, wild-type PLP2 mediated efficient cleavage of the nsp2|nsp3 junction (**Figure IV-3A**). As expected, a PLP2 active site mutant (C270A/H332A) did not display any processing of the nsp2|nsp3 site and only the nsp2-3 precursor was detected. Seven single-site mutants, in which the Ub-binding surface was targeted by replacement of Thr312 or Ile353, displayed wild-type levels of nsp2|nsp3 cleavage, suggesting that their polyprotein processing activity was not

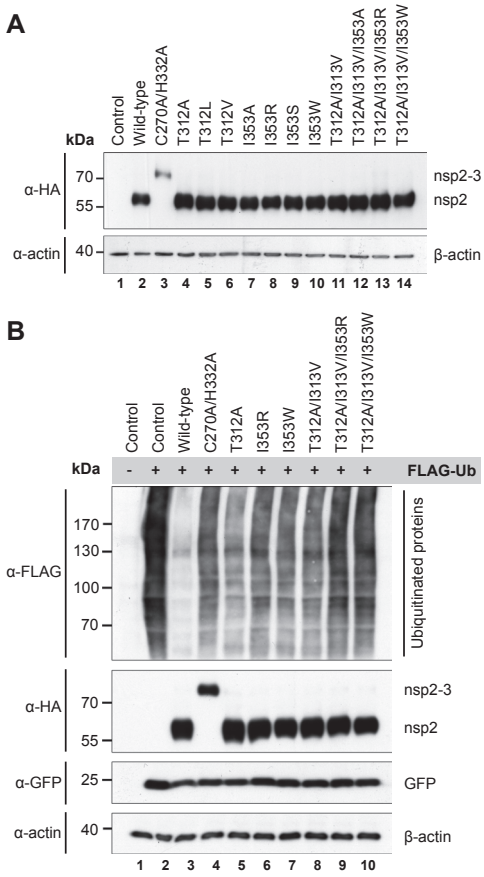

Figure IV-3: Decoupling of the polyprotein processing and DUB activities of EAV PLP2. A) HEK293T cells were transfected with plasmids encoding nsp2-3 containing wild-type or mutant PLP2. After 16 h at 37°C, cells were lysed and results were analyzed by Western blot. Proteolytic processing of the nsp2|nsp3 junction by wild-type PLP2 resulted in the release of HA-tagged nsp2 from the nsp2-3 precursor. **B)** HEK293T cells were transfected with a combination of plasmids encoding nsp2-3 containing wild-type or mutant PLP2 and FLAG-Ub. Expression of FLAG-Ub leads to FLAG-tagged ubiquitination of a wide range of cellular proteins, which can be visualized on Western blot using an anti-FLAG antibody. **Abbreviation:** Ub, ubiquitin.

notably affected. In addition, combinations of mutations at positions Thr312, Ile313, and Ile353 were tested, with similar results (**Figure IV-3A**). Longer exposure times did reveal some nsp2-3 precursor, even in the case of wild-type PLP2, but this amount only marginally increased when two or three mutations were combined (**Figure IV-4B**).

Next, we assayed the effect of these mutations on PLP2 DUB activity by transfecting mammalian cells with plasmids encoding FLAG-tagged Ub and nsp2-3 carrying wild-type or mutant PLP2. FLAG-tagged ubiquitination of a wide range of cellular targets could be visualized by Western blot analysis using an anti-FLAG antibody (**Figure IV-3B**). As expected, expression of wild-type PLP2 strongly decreased the accumulation of Ub-conjugates, while expression of the active site mutant (C270A/H332A) had a negligible effect. **Figure IV-3B** presents the results obtained with a selection of PLP2 Ub-binding surface mutants with the most pronounced effect on DUB activity, some of which approached the level of the active site mutant. In contrast, these Ub-binding

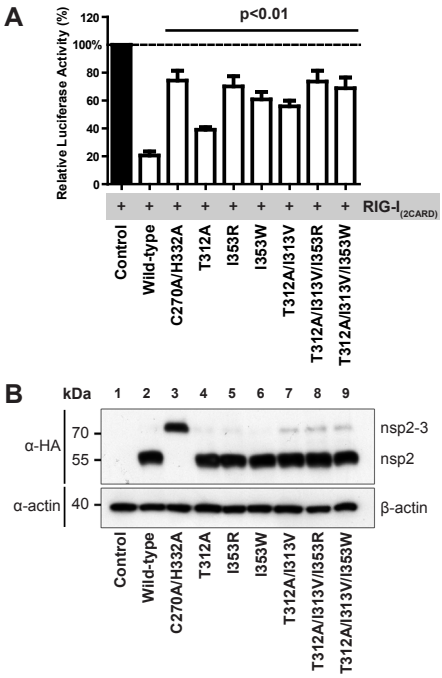

Figure IV-4: PLP2 Ub-binding surface mutations attenuate inhibition of IFN-β promoter activation. A) Luciferase-based reporter assay to assess the effect of various Ub-binding surface mutations on the inhibition of IFN-β promoter activity by PLP2. HEK293T cells were transfected with a combination of plasmids encoding firefly luciferase under control of the IFN-β promoter, renilla luciferase, RIG-$I_{(2CARD)}$, and nsp2-3 containing wild-type or mutant PLP2. Results were obtained in three independent experiments. Error bars represent standard deviations and p-values are relative to wild-type. **B)** Lysates obtained in each of the three experiments used for panel A were mixed in a 1:1:1 ratio and analyzed by Western blot for the expression of nsp2-3.

surface mutations had only minor effects on the deISGylating activity of PLP2 (**Figure IV-S1**).

To corroborate our findings from the expression system showing that PLP2 DUB activity could be selectively removed without disturbing nsp2|nsp3 cleavage, an *in vitro* activity assay of recombinant PLP2 produced in *E. coli* was performed using the fluorescently labeled substrates Ub-aminomethylcoumarin (Ub-AMC) or RLRGG-AMC, representing the C-terminal peptide motif of Ub. By comparing the activity of PLP2 mutants against Ub-AMC (which requires the Ub-binding surface) versus their activity against RLRGG-AMC (which binds to the active site region only), PLP2 mutants with a selective reduction in DUB activity could be identified. Indeed, compared to wild-type enzyme, mutants I353W and I353R exhibited ~10- and 20-fold reductions in specificity (k_{cat}/K_m) toward Ub, respectively; in contrast, their activity towards RLRGG-AMC was unaltered (**Table IV-1**). Expression of PLP2 containing additional mutations at Thr312 and Ile313 yielded insoluble protein in *E. coli*, preventing analysis of these mutants. Nevertheless, the results of the *in vitro* activity assay further confirmed the successful decoupling of the polyprotein processing and DUB activities of EAV PLP2 by specifically targeting key residues of the Ub-binding surface.

Table IV-1: Effect of Ub-binding surface mutations on the substrate specificity of PLP2.

PLP2 enzyme	Substrate	
	RLRGG-AMC	Ub-AMC
	k_{cat}/K_M	k_{cat}/K_M
Wild-type	45 ± 11 $M^{-1}s^{-1}$	17000 ± 4000 $M^{-1}s^{-1}$
I353R	65 ± 7 $M^{-1}s^{-1}$	413 ± 177 $M^{-1}s^{-1}$
I353W	155 ± 12 $M^{-1}s^{-1}$	1741 ± 850 $M^{-1}s^{-1}$

The ability of PLP2 to suppress innate immune signalling depends on its DUB activity. The effect of the various PLP2 Ub-binding surface mutations on innate immune signalling was initially assessed in the context of ectopic nsp2-3 expression using a luciferase-based IFN-β promoter activity assay. For this, HEK293T cells were transfected with a combination of plasmids encoding firefly luciferase under control of the IFN-β promoter, renilla luciferase as an endogenous control, constitutively active RIG-$I_{(2CARD)}$ to induce innate immune signalling (52), and EAV nsp2-3 containing either wild-type or mutant PLP2. In this assay, reporter gene expression was reduced to approximately 20% upon co-expression of wild-type PLP2, while 80% of the level of the untreated control was retained upon expression of the PLP2 active site mutant (C270A/H332A) (**Figure IV-4A**). Compared to wild-type PLP2, all mutants included in **Figure IV-4A** were significantly impaired in their inhibitory activity ($p<0.01$), with mutants I353R, I353W,

T312A/I313V/I353R, and T312A/I313V/I353W displaying inhibition levels similar to that of the active site mutant ($p>0.05$). Western blot analysis confirmed equal expression of wild-type and mutant nsp2-3 (**Figure IV-4B**). These results demonstrated that, at least in the context of the nsp2-3 expression system, the selective removal of PLP2 DUB activity significantly disrupted its ability to suppress IFN-β promoter activity.

Arteriviruses lacking PLP2 DUB activity elicit an enhanced host innate immune response. Having identified mutations in PLP2 that reduce its ability to suppress Ub-mediated innate immune signalling (**Figure IV-4A**) without adversely affecting nsp2|nsp3 cleavage (**Figure IV-3A**), we were in a position to directly evaluate the importance of PLP2 DUB activity for immune evasion during arterivirus infection. The six (combinations of) mutations used in **Figures IV-3B and 4** were introduced into an EAV full-length cDNA clone and mutant viruses were launched by electroporation of *in vitro* transcribed RNA into BHK-21 cells. Immunofluorescence microscopy subsequently confirmed expression of both nsp2 and the structural nucleocapsid (N) protein, followed by virus spread to initially untransfected cells. This indicated that viruses carrying these (combinations of) mutations were replication competent.

We next focused on the two mutants showing the greatest decrease in inhibitory activity in the IFN-β promoter activity assay: I353R and T312A/I313V/I353R (**Figure IV-4A**). We first characterized the replication kinetics of these mutants in a time-course experiment in primary equine lung fibroblasts (ELFs), which are derived from the natural host species of EAV and are likely to maintain an intact innate immune response. ELFs were infected with wild-type or mutant EAV at a multiplicity of infection (MOI) of 0.5 or 5. The first-cycle replication kinetics as determined by quantitative reverse transcriptase PCR (qRT-PCR) measurement of viral genome RNA levels did not notably differ between wild-type and mutant EAV (**Figures IV-5A and B**). In addition, viral titers in cell-culture supernatants harvested from infected ELFs at 24 h p.i. revealed no significant difference between wild-type and mutant EAV (**Figure IV-5C**). Finally, immunofluorescence microscopy of ELFs infected with MOI 5 revealed expression of nsp2 from 6 h p.i. onward, and by 9 h p.i. also expression of N protein could be seen in all cells for both wild-type and mutant EAV (**Figure IV-S2**). These results demonstrated that the replication kinetics of the PLP2 Ub-binding surface mutants and wild-type control were essentially the same, in line with our previous conclusion that cleavage of the nsp2|nsp3 site is hardly affected by these mutations. At the same time, Western blot analysis showed that, compared to wild-type EAV, the DUB activity of both mutants was severely impaired during infection (**Figure IV-5D**).

Subsequently, we used qRT-PCR to measure the levels of mRNAs encoding IFN-β, the IFN-stimulated protein MX1, and the pro-inflammatory cytokine IL8 and investigated the effect of mutations I353R and T312A/I313V/I353R on innate immune signalling

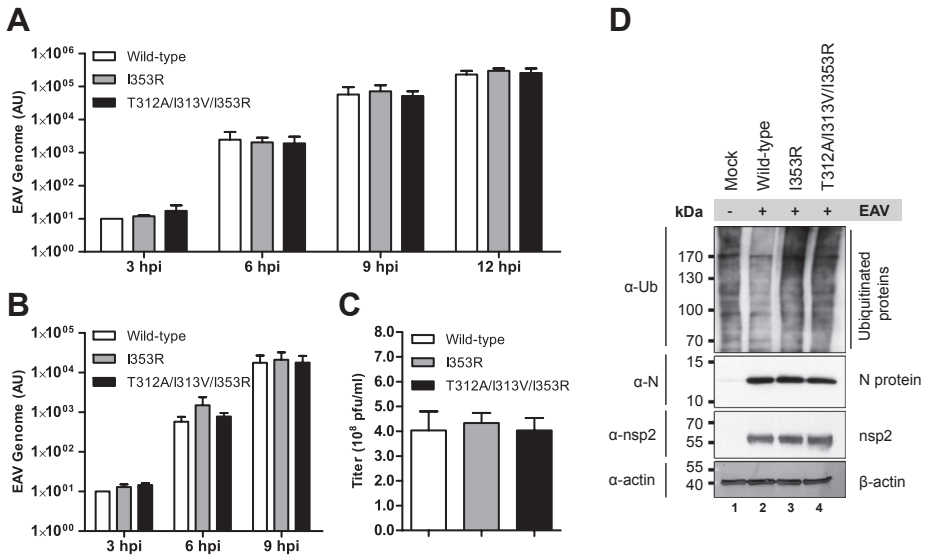

Figure IV-5: EAV PLP2 mutants display similar replication kinetics as wild-type virus. Equine lung fibroblasts were infected with wild-type or mutant EAV at MOI 0.5 (A) or 5 (B, C, D). **A and B)** At the indicated time-points, total RNA was isolated for qRT-PCR measurement of EAV genomic RNA levels. Results, which were obtained in three independent experiments, were analyzed using the standard curve method and normalized against the relative quantities of GAPDH and beta actin mRNA. Error bars represent standard deviations. **C)** At 24 h p.i., cell-culture supernatants were harvested and virus titers were determined by plaque assay on ELFs. Results were obtained in three independent experiments and error bars represent standard deviations. **D)** Cells were lysed at 10 h p.i. and total ubiquitination was assessed by Western blot analysis. **Abbreviations:** Ub, ubiquitin; N, nucleocapsid; hpi, hours post infection; AU, arbitrary units; pfu, plaque forming units.

during infection of ELFs. Initially, we infected ELFs with wild-type or mutant EAV at MOI 5, but in this set-up IFN-β mRNA levels remained below the detection limit at all time-points analyzed (from 3 to 12 h p.i.), suggesting that the innate immune response triggered by EAV upon initial infection is very limited. Therefore, we next infected ELFs with wild-type or mutant EAV at MOI 0.25, resulting in infection of about 20% of cells. We hypothesized that this would allow for IFN-β-mediated priming of uninfected cells as a result of paracrine signalling from cells infected during the first round. The expression of IFN-stimulated genes would then result in a more potent response during the second cycle of infection. Indeed, following such a low MOI infection with wild-type EAV, low but detectable levels of IFN-β mRNA were induced by 20 h p.i. (**Figure IV-6A**). Interestingly, at both 20 and 24 h p.i., cells infected with either mutant showed significantly increased levels of IFN-β mRNA compared to wild-type virus-infected cells ($p<0.05$), with mutant T312A/I313V/I353R showing the most pronounced difference. In addition, the levels of MX1 mRNA differed significantly between

wild-type and mutant EAV-infected cells at 24 h p.i. (**Figure IV-6B**). In contrast, at 20 and 24 h p.i., no significant difference in the levels of IL8 mRNA was observed upon infection with wild-type or mutant EAV (**Figure IV-6C**). Equally efficient replication of wild-type and mutant EAV was corroborated by comparing viral genome RNA levels, for which no significant differences were measured (**Figure IV-6D**). In summary, these data show that the PLP2 DUB function is indeed involved in the inhibition of innate immune signalling during EAV infection in primary equine cells and that it is possible to specifically inactivate this function to suppress immune evasion of otherwise fully replication-competent viruses.

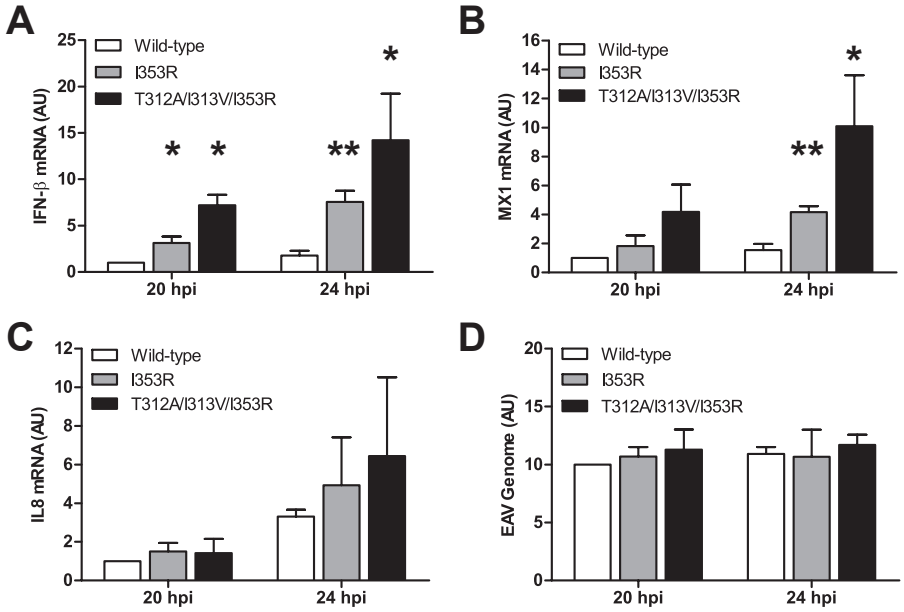

Figure IV-6: EAV lacking PLP2 DUB activity elicits an enhanced innate immune response. Equine lung fibroblasts were infected with EAV encoding wild-type or mutant PLP2 at MOI 0.25 and at 20 and 24 h p.i. RNA was isolated for qRT-PCR measurement of the levels of **A)** IFN-β mRNA, **B)** MX1 mRNA, **C)** IL8 mRNA, or **D)** EAV genomic RNA. Results, which were obtained in three independent experiments, were analyzed using the standard curve method and normalized against the relative quantities of GAPDH and beta actin mRNA. Error bars represent standard deviation and asterisks indicate a significant difference relative to wild-type at the same time-point. * $p<0.05$; ** $p<0.01$. **Abbreviations:** AU, arbitrary units; hpi, hours post infection.

DISCUSSION

Due to the widespread adoption of polyprotein synthesis and cleavage as a genome expression strategy in +RNA viruses and retroviruses, proteases have become key regulatory enzymes of the replication of many important human and animal pathogens. Moreover, virus-host co-evolution has offered ample opportunity to develop additional protease functions, which promote virus replication by targeting cellular rather than viral substrates. Since both functions depend on the same protease active site, it has been intrinsically difficult to study them independently during virus infection, mainly because protease inactivation *per se* is generally incompatible with virus viability. The independent assessment of the cleavage of host cell targets requires its decoupling from viral polyprotein processing, which to date has only been achieved for the poliovirus 2A protease (53-56). Our present work on EAV PLP2 illustrates how structure-guided mutagenesis can be applied to specifically disrupt the interaction of a viral protease with its cellular substrate. The identification of a Ub-binding surface that is distant from the PLP2 active site, allowed us to specifically inactivate the DUB function of the enzyme and - ultimately - probe its relevance in the context of the infected cell. Compared to wild-type EAV, viruses that lack PLP2 DUB activity induced a significantly enhanced innate immune response in primary equine cells, while displaying essentially identical replication kinetics, thus demonstrating the importance of this activity in the evasion of innate immune signalling by arteriviruses.

Analysis of the EAV PLP2 fold using the DALI server identified members of the OTU superfamily as its closest structural relatives, supporting its classification as a member of this superfamily. However, the limited sequence similarity between arterivirus PLP2 and other OTU proteases was previously rated as statistically insignificant (29) and our structure reveals topological features that deviate considerably from a typical OTU-fold. Domain I of known OTU-domain structures contains a pair of solvent exposed α-helices that pack perpendicularly against two internal helices (**Figures IV-1E, G, and H**). While the internal helices are conserved in PLP2 (α1 and α2), the solvent exposed helices have been replaced by a single helix (α4) that packs parallel to helices α1 and α2 to form a three-helix bundle that comprises most of domain I (**Figures IV-1E and F**). This topology subtly resembles the L domain of papain (57) and markedly reduces the size of domain I and its contribution to Ub binding relative to other OTU DUBs that have been determined in complex with Ub (38, 43-45, 48). The compact fold of arterivirus PLP2 may be required for its function in replicase polyprotein maturation, an activity that is not shared by cellular OTU DUBs or the OTU protease of CCHFV (58).

A more striking deviation from known OTU-domain structures is the presence of the zinc finger in PLP2 domain II (**Figure IV-1C**) and its critical importance for catalytic

activity (16). Ub-binding domains that contain zinc fingers exist within a number of OTU DUBs, but none comprise part of the distal Ub-binding site within the OTU-fold. Instead, they exist as accessory domains that are connected to the OTU-domain through flexible linkers (42), where, in the case of A20, they appear to provide additional polyubiquitin linkage specificity and possibly target the protein to specific signalling complexes (59). For PLP2, the zinc finger is an integral part of the OTU-fold and it plays a central role in binding and positioning the distal Ub molecule on the protease surface (**Figure IV-2A**). Currently, OTU DUBs are grouped into three subclasses based on their structural characteristics: the Otubains, the A20-like OTU's, and the OTU's (42). Given the unique features of EAV PLP2, we propose that arterivirus PLP2 enzymes represent a new, fourth subclass of zinc-dependent OTU's.

We believe that the structure-guided inactivation of the PLP2 DUB function may contribute to the engineering of improved modified live vaccines (MLVs) for arteriviruses. Although generally effective strategies for the prevention and control of equine viral arteritis have been developed, several field strains are poorly neutralized by antibodies from horses vaccinated with the ARVAC vaccine strain (60) and EAV outbreaks continue to cause significant disruptions of the horse breeding industry (61). While our current work focuses on EAV PLP2, the corresponding protease of PRRSV has been shown to have very similar immune evasive properties in a variety of experimental settings (18, 30, 31). Since its discovery in the late 1980s, PRRSV has spread around the globe and now ranks among the most important swine pathogens. PRRSV infection causes annual losses of approximately $664 million in the United States alone (62) and the emergence of highly virulent strains in China is of particular concern (63-65). Moreover, the virus has proven difficult to control and it has been suggested to counteract innate immunity, thus undermining the overall immune response and viral clearance in infected animals (66). Consequently, inactivation of the PLP2 DUB function may be an important step in the design of improved vaccine candidates. These should induce a more robust innate response and, therefore, also a more potent adaptive immune reaction than that achieved with the currently available MLVs. Multiple studies have suggested that additional arterivirus nsps may contribute to innate immune evasion (67, 68) and, consequently, vaccine efficacy may be further bolstered by targeting a combination of such functions. As in this study, detailed insight into the molecular interactions of these other arterivirus proteins and their host ligands will likely be required to achieve this goal without crippling the basic replication capacity of the virus. In cell culture, our most promising EAV PLP2 mutant, carrying mutations T312A/I313V/I353R, induced an approximately 8-fold increase in IFN-β mRNA levels compared to wild-type virus. Although we were unable to investigate this effect *in vivo* due to the lack of a small animal model for EAV infection, the disabling of immune

evasion mechanisms can result in significant virus attenuation. One striking example is the modification of the immune evasive influenza virus NS1 protein, which yielded attenuated viruses that are promising vaccine candidates (69).

In addition to opening new possibilities for vaccine development, the mutants described in this paper should provide excellent tools for identifying the cellular targets of PLP2, which to date remain unknown. Although Western blot analysis suggests that PLP2 acts in a very promiscuous fashion, causing a general decrease in the levels of ubiquitinated host proteins (**Figure IV-5D**), our qRT-PCR results support the idea that there is at least some degree of specificity in the inhibition of innate immune signalling, as evidenced by the PLP2-mediated inhibition of IFN-β mRNA transcription, but not IL8 mRNA transcription (**Figures IV-6A, C**). Since the expression of IFN-β depends largely on the activation of the transcription factor IRF3 and expression of pro-inflammatory cytokines like IL8 does not (27), our findings suggest that PLP2-mediated inhibition of innate immunity is primarily directed at IRF3-dependent signalling. Future experiments will aim at elucidating the target specificity of arterivirus PLP2.

Arteriviruses are not the only virus family harboring proteases with multiple substrate specificities. Especially interesting in this respect are the distantly related coronaviruses (CoV), which infect a wide variety of species, including livestock, companion animals, bats, and humans. Six CoV species have now been found to infect humans, causing symptoms ranging from mild respiratory illness to acute respiratory syndromes, as in the case of SARS-CoV (70) and the recently emerged HCoV-EMC/2012 (71, 72). The replicase polyproteins of coronaviruses harbor one or two papain-like proteases (PLpro's) that participate in polyprotein maturation and presumably promote evasion of innate immunity by means of their DUB activity (32, 34, 37, 73). Although the CoV PLpro's belong to the Ub-specific protease (USP) (74, 75) rather than the OTU superfamily of DUBs, it is likely that also coronavirus PLpro substrate specificities can be decoupled using a similar structure-guided approach. Here we have illustrated how structure-guided mutagenesis of such a viral protease may be used to enhance the innate immune response to infection, a strategy that may be applied in the design of MLVs targeting arteriviruses and other virus families encoding similar dual-specificity proteases.

MATERIALS AND METHODS

Plasmids, cells, and antibodies

The following mammalian expression plasmids were described elsewhere: pLuc-IFN-β (76), pRL-TK (Promega), pEBG-RIG-$I_{(2CARD)}$ (52), pcDNA-eGFP (31), pCMV-FLAG-Ub (77), pCAGGS-HA-mUbE1L, pCMV2-FLAG-UbcM8, and pCAGGS-V5-hISG15 (78).

HEK293T cells were cultured in Dulbecco's modified Eagle medium (Lonza) supplemented with 10% fetal bovine serum (FBS), and 2 mM L-glutamine. BHK-21 cells were cultured in Glasgow minimum essential medium (Lonza) supplemented with 5% FBS, 10% tryptose phosphate broth, and 10 mM HEPES (pH 7.4). Primary equine lung fibroblasts (ELF) were cultured in minimum essential medium (Lonza) supplemented with 10% FBS and grown on collagen-coated plastics. All culture media contained 100 U/ml of penicillin and 100 mg/ml of streptomycin.

The following commercially available antibodies were used: α-HA (ab18181; Abcam), α-FLAG (F3165; Sigma-Aldrich), α-GST (sc459; Santa Cruz), α-ubiquitin (#3933; Cell Signaling Technology), α-β-actin (A5316; Sigma-Aldrich), donkey-α-mouse-Cy3 (715-165-151; Jackson ImmunoResearch), and goat-α-rabbit-AL488 (A-11008; Invitrogen). The following antibodies were described elsewhere: α-EAV N protein (clone 3E2) (79) and α-ISG15 (clone 2.1) (80). Rabbit antiserum recognizing the C-terminus of EAV nsp2 was raised using a mix of two peptides (ASTVDPHSFDQKK and GDFLKLNPGFRLIGG) and rabbit antiserum recognizing GFP was raised using recombinant protein purified from *Escherichia coli*.

PLP2 plasmids

For bacterial expression of EAV PLP2, a cDNA fragment encoding residues 261-392 of EAV pp1a and an in-frame C-terminal His_6 purification tag was inserted downstream of a Ub fusion partner in the pASK3 vector (81), yielding plasmid pASK3-ePLP2. A mammalian expression construct encoding an EAV nsp2-3 polyprotein was made by cloning residues 261-1064 of EAV pp1a in-frame with an N-terminal HA tag in the pcDNA3.1 vector (Invitrogen). All mutants were engineered by site-directed mutagenesis using *Pfu* DNA polymerase (Fermentas). Primer sequences are available upon request. All constructs were verified by sequence analysis.

Purification and crystallization of EAV PLP2 bound to Ub

E. coli BL21-Gold(DE3) cells were transformed with pASK3-ePLP2 and cultured to an optical density (OD_{600}) of 0.7 in LB medium at 37°C. The culture was then supplemented with 200 ng/ml of anhydrous tetracycline and incubated for 3 h at 28°C with shaking to induce expression of the Ub-PLP2-His_6 fusion protein. The cells were pelleted and resuspended in ice-cold lysis buffer (20 mM MES pH 7, 500 mM NaCl, 10% glycerol, 5

mM imidazole pH 7.4, 0.5 mM TCEP) and lysed using a French pressure cell (AMECO). The lysate was clarified by centrifugation and loaded onto a Ni-NTA column (Qiagen) pre-equilibrated with lysis buffer. After washing with lysis buffer supplemented with 15 mM imidazole, recombinant PLP2 was eluted from the column using an equilibration buffer supplemented with 150 mM imidazole and exchanged into 50 mM Tris, pH 8.0, 300 mM NaCl and 5 mM DTT before storing at 4 °C. The endogenous DUB activity of PLP2 resulted in the efficient removal of the N-terminal Ub-tag from the fusion protein during expression in *E. coli*; therefore, affinity chromatography yielded highly pure PLP2 carrying a C-terminal His_6 purification tag only.

The mechanism-based suicide inhibitor $Ub_{(1-75)}$–3–bromopropylamine (Ub–3Br) was prepared according to Messick *et al* (38) and Borodovsky *et al* (39), as described by James *et al* (43). Ub-3Br was covalently bound to purified PLP2 by gently mixing the proteins in a 3:2 molar ratio for one hour at 37°C. The resulting PLP2-Ub complex was purified by gel filtration (Superdex 75) followed by anion exchange (Source 15Q) chromatography and then exchanged into 20 mM Tris, pH 8.0, 50 mM NaCl before concentrating to 10 mg/ml and storing at 4°C.

The PLP2-Ub complex was crystallized by hanging-drop vapor diffusion at 10 mg/ml in mother liquor consisting of 100 mM MES pH 6.2, 18% PEG 20,000. Crystals were flash-cooled and stored in liquid nitrogen after sweeping them through mother liquor supplemented with 20% glycerol.

X-ray data collection and crystal structure determination

X-ray diffraction data for a multiwavelength anomalous dispersion (MAD) experiment were collected at the Canadian Light Source (beam line 08ID-1). Data were collected at three different wavelengths over the absorption edge of zinc from a single crystal of the PLP2-Ub complex held at 100K in a N_2 (g) stream. The data were processed using MOSFLM and SCALA (82) and structure factor phases were determined using phenix.autosol (83). Initial phases generated by SOLVE were improved by density modification using RESOLVE within the PHENIX package. After reserving a random subset of reflections for cross-validation using the free R-factor (84), a model was built using phenix.autobuild (83) and manually completed and refined using COOT (85) and phenix.refine (83). Crystallographic data and model refinement statistics are summarized in **Table IV-S1**.

In vitro enzymatic assays

The DUB activity of PLP2 (wild type and mutants) was assayed using 7-amino-4-methylcoumarin (AMC) labelled versions of Ub (Ub-AMC) (Boston Biochem) and the C-terminal peptide motif of Ub, RLRGG-AMC (Enzo Life Sciences). The enzymes cleave the AMC label causing a significant increase in the fluorescence quantum yield of the

dye. All reactions were performed in 20 mM tris-Cl buffer at pH 8 and 100 mM NaCl. Time-dependent fluorescence traces were collected by a Fluorolog-3 Horiba Jobin Yvon fluorimeter. The monochromators were set to 360 nm (excitation) and to 460 nm (emission). The slits were set between 1-3 nm bandpass depending on substrate concentration. Enzyme activities in all mutants were characterized by the specificity constant $\frac{k_{cat}}{K_m}$. At substrate concentrations significantly smaller than K_m the formation of product follows pseudo-first-order kinetics, therefore the temporal evolution of product fluorescence F follows the equation:

$$F=F_{\infty}\left(1-\exp\left(-\frac{k_{cat}[E]}{K_m}t\right)\right)+F_0 \quad (1)$$

Where F_{∞} is the fluorescence when all AMC is liberated, F_0 is the background fluorescence, $[E]$ is the total enzyme concentration and t is the time elapsed. From fitting the fluorescence time traces to equation 1, all parameters including the specificity constant $\frac{k_{cat}}{K_m}$ are obtained. Our assays indicate that PLP2 exhibits pseudo-first-order kinetics for Ub-AMC at concentrations less than 0.2 μM and for RLRGG-AMC at concentrations less than 150 μM.

Cell culture-based assays

To assess nsp2|3 cleavage by the various PLP2 mutants, HEK293T cells were grown to 80% confluence in 10 cm^2 wells and transfected using $CaPO_4$ with 4 μg plasmid DNA encoding nsp2-3 containing wild-type or mutant PLP2. After 16 h at 37°C, cells were lysed in 2x Laemmli Sample Buffer (2xLSB; 250 mM Tris, 2% SDS, 20% glycerol, 0.01% bromophenol blue, 2 mM DTT, pH 6.8). Samples were loaded on SDS-polyacrylamide gels, which were blotted to Hybond-P polyvinylidene difluoride membranes (GE Healthcare) using a semi-dry transfer cell (Bio-Rad). After incubation with the appropriate antibodies, protein bands were visualized using the Amersham ECL Plus detection reagent (GE Healthcare).

To assess the DUB activity of the various PLP2 mutants, HEK293T cells were grown to 80% confluence in 4 cm^2 wells and transfected using $CaPO_4$ with a combination of plasmids encoding FLAG-Ub (0.25 μg), GFP (0.25 μg), and nsp2-3 containing wild-type or mutant PLP2 (1.5 μg). After 16 h at 37°C, cells were lysed in 2xLSB and analyzed by SDS-PAGE as described above.

To assess the deISGylation activity of the various mutants, HEK293T cells were grown to 80% confluence in 12-well plates and transfected using $CaPO_4$ with a combination of plasmids encoding hISG15 (0.75 μg), HA-mUbE1L (0.25 μg), FLAG-UbcM8 (0.25 μg), GFP (0.25 μg) and wild-type or mutant nsp2-3 (0.5 μg). After 48 h at 37°C, cells were lysed in 2xLSB and analyzed by SDS-PAGE as described above.

Luciferase-based IFN-β promoter activity assay

HEK293T cells, grown to 80% confluence in 2 cm^2 wells, were transfected in quadruplicate with a combination of plasmids encoding firefly luciferase under control of the IFN-β promoter (50 ng), renilla luciferase (5 ng), RIG-$I_{(2CARD)}$ (25 ng) and nsp2-3 containing wild-type or mutant PLP2 (500 ng) using Lipofectamine2000 (Invitrogen). The total amount of DNA used for transfection was adjusted to 1 µg per well by the addition of the appropriate amount of empty vector. After 12 h at 37°C, three out of four wells were lysed in 100 µl passive lysis buffer (Promega), and samples were assayed for luciferase activity using the Dual-Luciferase reporter assay system (Promega) on a Mithras LB 940 multimode reader (Berthold Technologies). The remaining wells from each of three independent experiments were lysed in 2xLSB, mixed in a 1:1:1 ratio and analyzed by SDS-PAGE as described above. Using SPSS Statistics software, an unpaired two-tailed Student's *t* test was used to determine the statistical significance of the results, which were obtained in three independent experiments. P values <0.05 were considered to be statistically significant.

Reverse genetics

Mutations in the EAV PLP2-coding sequence were engineered in an appropriate shuttle vector and subsequently transferred to pEAN551/AB, a derivative of EAV full-length cDNA clone pEAN551 carrying additional (translationally silent) *Afl*II and *Bsp*EI restriction sites (17, 86). The virus derived from pEAN551/AB was used as wild-type control in all experiments. All constructs were verified by sequence analysis.

In vitro RNA transcription from *Xho*I-linearized wild-type or mutant EAV full-length cDNA clones was performed using the mMESSAGE mMACHINE T7 Kit (Ambion). Five µg of full-length EAV RNA was electroporated into $5.0*10^6$ BHK-21 cells using the Amaxa Cell Line Nucleofector Kit T and the program T-020 of the Amaxa Nucleofector (Lonza) according to the manufacturer's instructions. Cells were incubated at 39.5°C and virus-containing supernatants were harvested at 24 h post transfection. Titers were determined by plaque assay on primary equine lung fibroblasts (ELFs) essentially as described before (87).

To verify the presence of the correct mutations, RNA was isolated from virus-containing supernatants using the QIAamp Viral RNA Mini Kit (Qiagen) and converted to cDNA using RevertAid H Minus reverse transcriptase (Fermentas) and random hexameric primers. The region of PLP2 encoding the mutations was subsequently PCR amplified using *Pfu* DNA polymerase (Fermentas) and sequenced.

Immunofluorescence microscopy

Confluent ELFs were infected with wild-type or mutant EAV at a multiplicity of infection (MOI) of 5 and incubated at 37°C. At 3, 6, and 9 h post infection (p.i.), cells were

fixed with 3% paraformaldehyde in phosphate buffered saline (PBS; pH 7.4). Following permeabilization in 0.2% Triton X-100 in PBS, EAV nsp2 and N protein were visualized by indirect immunofluorescence microscopy using the appropriate antibodies. Specimens were examined with a Zeiss Axioskop 2 fluorescence microscope with an Axiocam HRc camera and Zeiss Axiovision 4.2 software.

Quantitative reverse transcriptase PCR

Confluent ELFs were infected with wild-type or mutant EAV at MOI 5, 0.5, or 0.25 and incubated at 37°C. At the indicated time-points, cell lysates were harvested in TriPure Isolation Reagent (Roche). After the addition of chloroform, the aqueous phase was mixed in a 1:1 ratio with buffer RA1 of the Nucleospin RNA II kit (Macherey-Nagel). RNA was isolated as per manufacturer's instructions and reverse transcribed using RevertAid H Minus RT (Fermentas) and oligo(dT)$_{20}$ primer. Finally, samples were assayed by quantitative reverse transcriptase PCR (qRT-PCR) on a CFX384 Touch Real-Time PCR detection system (BioRad) using iTaq SYBR Green Supermix with ROX (BioRad). Primers (see **Table IV-S2**) targeting mRNAs encoding equine GAPDH, Actin-β, IFN-β, MX1, and the EAV genome were designed using Primer3 (88) or kindly provided by Udeni Balasuriya in the case of IL8. The real-time PCR was followed by a melting-curve analysis, to verify the specificity of the reaction. Results were quantified using the standard curve method and normalized against the geometric mean of the relative quantities of GAPDH and Actin-β mRNA. Data from three independent experiments was analyzed with SPSS Statistics software using a one-sample *t* test or unpaired Student's *t* test, where appropriate. P values <0.05 were considered to be statistically significant.

Deubiquitination during infection

Confluent ELFs were infected with wild-type or mutant EAV at MOI 5 and incubated for 10 hours at 37°C. Cells were then lysed in 500 µl 2x Laemmli Sample Buffer (250 mM Tris, 2% SDS, 20% glycerol, 0.01% bromophenol blue, 2 mM DTT, pH 6.8) and total ubiquitination was assessed by Western blot analysis as described in the supplemental materials and methods section.

Atomic coordinates

Atomic coordinates and structure factors for the PLP2-Ub complex have been deposited in the Protein Data Bank under the accession code: 4IUM.

ACKNOWLEDGEMENTS

We thank Adolfo García-Sastre, John-Paul Bacik, John Hiscott, Udeni B. Balasuriya, Alexander E. Gorbalenya, Aartjan J.W. te Velthuis, Adriaan H. de Wilde, Kathleen C. Lehman, and Diede Oudshoorn for helpful discussions. We thank V. Larmour for technical assistance and S. Labiuk and the staff of the Canadian Light Source (CLS) beamline 08ID-1 for assistance with data collection. The CLS is supported by NSERC, the National Research Council, the Canadian Institutes of Health Research (CIHR), and the University of Saskatchewan. We kindly thank the following people for providing us with reagents: Erwin van den Born, Craig E. Cameron, Natalia Frias-Staheli, Michaela U. Gack, Paul N. Moynagh, Adolfo García-Sastre and Gijs A. Versteeg.

This research was supported in part by the Division of Chemical Sciences of the Netherlands Organization for Scientific Research (NWO-CW) through ECHO grant 700.59.008 to M.K. and E.J.S., and by a Natural Sciences and Engineering Research Council of Canada (NSERC) grant. B.L.M. holds a Manitoba Research Chair award. The research was also supported in part by the European Union Seventh Framework Programme (FP7/2007-2013) under SILVER grant agreement no. 260644.

REFERENCES

1. **Firth AE, Brierley I.** 2012. Non-canonical translation in RNA viruses. J Gen Virol **93:**1385-1409.
2. **Dougherty WG, Semler BL.** 1993. Expression of virus-encoded proteinases: functional and structural similarities with cellular enzymes. Microbiol Rev **57:**781-822.
3. **Gorbalenya AE, Donchenko AP, Blinov VM, Koonin EV.** 1989. Cysteine proteases of positive strand RNA viruses and chymotrypsin-like serine proteases. A distinct protein superfamily with a common structural fold. FEBS letters **243:**103-114.
4. **Gorbalenya AE, Koonin EV, Lai MM.** 1991. Putative papain-related thiol proteases of positive-strand RNA viruses. Identification of rubi- and aphthovirus proteases and delineation of a novel conserved domain associated with proteases of rubi-, alpha- and coronaviruses. FEBS letters **288:**201-205.
5. **Hellen CU, Krausslich HG, Wimmer E.** 1989. Proteolytic processing of polyproteins in the replication of RNA viruses. Biochemistry **28:**9881-9890.
6. **Etchison D, Milburn SC, Edery I, Sonenberg N, Hershey JW.** 1982. Inhibition of HeLa cell protein synthesis following poliovirus infection correlates with the proteolysis of a 220,000-dalton polypeptide associated with eucaryotic initiation factor 3 and a cap binding protein complex. J Biol Chem **257:**14806-14810.
7. **Krausslich HG, Nicklin MJ, Toyoda H, Etchison D, Wimmer E.** 1987. Poliovirus proteinase 2A induces cleavage of eucaryotic initiation factor 4F polypeptide p220. J Virol **61:**2711-2718.
8. **Li XD, Sun L, Seth RB, Pineda G, Chen ZJ.** 2005. Hepatitis C virus protease NS3/4A cleaves mitochondrial antiviral signalling protein off the mitochondria to evade innate immunity. Proc Natl Acad Sci U S A **102:**17717-17722.
9. **Meylan E, Curran J, Hofmann K, Moradpour D, Binder M, Bartenschlager R, Tschopp J.** 2005. Cardif is an adaptor protein in the RIG-I antiviral pathway and is targeted by hepatitis C virus. Nature **437:**1167-1172.
10. **Ventoso I, MacMillan SE, Hershey JW, Carrasco L.** 1998. Poliovirus 2A proteinase cleaves directly the eIF-4G subunit of eIF-4F complex. FEBS letters **435:**79-83.
11. **Balasuriya UB, MacLachlan NJ.** 2004. The immune response to equine arteritis virus: potential lessons for other arteriviruses. Vet Immunol Immunopathol **102:**107-129.
12. **Huang YW, Meng XJ.** 2010. Novel strategies and approaches to develop the next generation of vaccines against porcine reproductive and respiratory syndrome virus (PRRSV). Virus Res **154:**141-149.
13. **Fang Y, Snijder EJ.** 2010. The PRRSV replicase: exploring the multifunctionality of an intriguing set of nonstructural proteins. Virus Res **154:**61-76.
14. **Ziebuhr J, Snijder EJ, Gorbalenya AE.** 2000. Virus-encoded proteinases and proteolytic processing in the Nidovirales. J Gen Virol **81:**853-879.
15. **Han J, Rutherford MS, Faaberg KS.** 2009. The porcine reproductive and respiratory syndrome virus nsp2 cysteine protease domain possesses both trans- and cis-cleavage activities. J Virol **83:**9449-9463.
16. **Snijder EJ, Wassenaar AL, Spaan WJ, Gorbalenya AE.** 1995. The arterivirus Nsp2 protease. An unusual cysteine protease with primary structure similarities to both papain-like and chymotrypsin-like proteases. J Biol Chem **270:**16671-16676.

17. **Posthuma CC, Pedersen KW, Lu Z, Joosten RG, Roos N, Zevenhoven-Dobbe JC, Snijder EJ.** 2008. Formation of the arterivirus replication/transcription complex: a key role for nonstructural protein 3 in the remodeling of intracellular membranes. J Virol **82:**4480-4491.
18. **Frias-Staheli N, Giannakopoulos NV, Kikkert M, Taylor SL, Bridgen A, Paragas J, Richt JA, Rowland RR, Schmaljohn CS, Lenschow DJ, Snijder EJ, Garcia-Sastre A, Virgin HWt.** 2007. Ovarian tumor domain-containing viral proteases evade ubiquitin- and ISG15-dependent innate immune responses. Cell Host Microbe **2:**404-416.
19. **Behrends C, Harper JW.** 2011. Constructing and decoding unconventional ubiquitin chains. Nat Struct Mol Biol **18:**520-528.
20. **Komander D.** 2009. The emerging complexity of protein ubiquitination. Biochemical Society transactions **37:**937-953.
21. **Enesa K, Zakkar M, Chaudhury H, Luong le A, Rawlinson L, Mason JC, Haskard DO, Dean JL, Evans PC.** 2008. NF-kappaB suppression by the deubiquitinating enzyme Cezanne: a novel negative feedback loop in pro-inflammatory signalling. J Biol Chem **283:**7036-7045.
22. **Kayagaki N, Phung Q, Chan S, Chaudhari R, Quan C, O'Rourke KM, Eby M, Pietras E, Cheng G, Bazan JF, Zhang Z, Arnott D, Dixit VM.** 2007. DUBA: a deubiquitinase that regulates type I interferon production. Science **318:**1628-1632.
23. **Li S, Zheng H, Mao AP, Zhong B, Li Y, Liu Y, Gao Y, Ran Y, Tien P, Shu HB.** 2010. Regulation of virus-triggered signalling by OTUB1- and OTUB2-mediated deubiquitination of TRAF3 and TRAF6. J Biol Chem **285:**4291-4297.
24. **Wertz IE, O'Rourke KM, Zhou H, Eby M, Aravind L, Seshagiri S, Wu P, Wiesmann C, Baker R, Boone DL, Ma A, Koonin EV, Dixit VM.** 2004. De-ubiquitination and ubiquitin ligase domains of A20 downregulate NF-kappaB signalling. Nature **430:**694-699.
25. **Jiang X, Chen ZJ.** 2012. The role of ubiquitylation in immune defence and pathogen evasion. Nat Rev Immunol **12:**35-48.
26. **Oudshoorn D, Versteeg GA, Kikkert M.** 2012. Regulation of the innate immune system by ubiquitin and ubiquitin-like modifiers. Cytokine Growth Factor Rev **23:**273-282.
27. **Jensen S, Thomsen AR.** 2012. Sensing of RNA viruses - A review on innate immune receptors involved in recognizing RNA virus invasion. J Virol 86:2900-2910.
28. **O'Neill LA, Bowie AG.** 2010. Sensing and signalling in antiviral innate immunity. Curr Biol **20:**R328-333.
29. **Makarova KS, Aravind L, Koonin EV.** 2000. A novel superfamily of predicted cysteine proteases from eukaryotes, viruses and Chlamydia pneumoniae. Trends Biochem Sci **25:**50-52.
30. **Sun Z, Chen Z, Lawson SR, Fang Y.** 2010. The cysteine protease domain of porcine reproductive and respiratory syndrome virus nonstructural protein 2 possesses deubiquitinating and interferon antagonism functions. J Virol **84:**7832-7846.
31. **van Kasteren PB, Beugeling C, Ninaber DK, Frias-Staheli N, van Boheemen S, Garcia-Sastre A, Snijder EJ, Kikkert M.** 2012. Arterivirus and Nairovirus Ovarian Tumor Domain-Containing Deubiquitinases Target Activated RIG-I To Control Innate Immune Signaling. J Virol **86:**773-785.
32. **Devaraj SG, Wang N, Chen Z, Tseng M, Barretto N, Lin R, Peters CJ, Tseng CT, Baker SC, Li K.** 2007. Regulation of IRF-3-dependent innate immunity by the papain-like protease

domain of the severe acute respiratory syndrome coronavirus. J Biol Chem **282:**32208-32221.

33. **Inn KS, Lee SH, Rathbun JY, Wong LY, Toth Z, Machida K, Ou JH, Jung JU.** 2011. Inhibition of RIG-I-mediated signalling by Kaposi's sarcoma-associated herpesvirus-encoded deubiquitinase ORF64. J Virol **85:**10899-10904.
34. **Frieman M, Ratia K, Johnston RE, Mesecar AD, Baric RS.** 2009. Severe acute respiratory syndrome coronavirus papain-like protease ubiquitin-like domain and catalytic domain regulate antagonism of IRF3 and NF-kappaB signalling. J Virol **83:**6689-6705.
35. **Jiang J, Tang H.** 2010. Mechanism of inhibiting type I interferon induction by hepatitis B virus X protein. Protein Cell **1:**1106-1117.
36. **Wang D, Fang L, Li P, Sun L, Fan J, Zhang Q, Luo R, Liu X, Li K, Chen H, Chen Z, Xiao S.** 2011. The leader proteinase of foot-and-mouth disease virus negatively regulates the type I interferon pathway by acting as a viral deubiquitinase. J Virol **85:**3758-3766.
37. **Zheng D, Chen G, Guo B, Cheng G, Tang H.** 2008. PLP2, a potent deubiquitinase from murine hepatitis virus, strongly inhibits cellular type I interferon production. Cell Res **18:**1105-1113.
38. **Messick TE, Russell NS, Iwata AJ, Sarachan KL, Shiekhattar R, Shanks JR, Reyes-Turcu FE, Wilkinson KD, Marmorstein R.** 2008. Structural basis for ubiquitin recognition by the Otu1 ovarian tumor domain protein. J Biol Chem **283:**11038-11049.
39. **Borodovsky A, Ovaa H, Kolli N, Gan-Erdene T, Wilkinson KD, Ploegh HL, Kessler BM.** 2002. Chemistry-based functional proteomics reveals novel members of the deubiquitinating enzyme family. Chem Biol **9:**1149-1159.
40. **Andreini C, Bertini I, Cavallaro G.** 2011. Minimal Functional Sites Allow a Classification of Zinc Sites in Proteins. PLoS One **6:**e26325.
41. **Holm L, Rosenström P.** 2010. Dali server: conservation mapping in 3D. Nucleic Acids Research **38:**W545-W549.
42. **Komander D, Clague MJ, Urbe S.** 2009. Breaking the chains: structure and function of the deubiquitinases. Nat Rev Mol Cell Biol **10:**550-563.
43. **James TW, Frias-Staheli N, Bacik JP, Levingston Macleod JM, Khajehpour M, Garcia-Sastre A, Mark BL.** 2011. Structural basis for the removal of ubiquitin and interferon-stimulated gene 15 by a viral ovarian tumor domain-containing protease. Proc Natl Acad Sci U S A **108:**2222-2227.
44. **Akutsu M, Ye Y, Virdee S, Chin JW, Komander D.** 2011. Molecular basis for ubiquitin and ISG15 cross-reactivity in viral ovarian tumor domains. Proc Natl Acad Sci U S A **108:**2228-2233.
45. **Capodagli GC, McKercher MA, Baker EA, Masters EM, Brunzelle JS, Pegan SD.** 2011. Structural analysis of a viral ovarian tumor domain protease from the Crimean-Congo hemorrhagic fever virus in complex with covalently bonded ubiquitin. J Virol **85:**3621-3630.
46. **Juang Y-C, Landry M-C, Sanches M, Vittal V, Leung CCY, Ceccarelli Derek F, Mateo A-Rachele F, Pruneda Jonathan N, Mao DYL, Szilard Rachel K, Orlicky S, Munro M, Brzovic PeterS, Klevit RachelE, Sicheri F, Durocher D.** 2012. OTUB1 Co-opts Lys48-Linked Ubiquitin Recognition to Suppress E2 Enzyme Function. Molecular Cell **45:**384-397.
47. **Wiener R, Zhang X, Wang T, Wolberger C.** 2012. The mechanism of OTUB1-mediated inhibition of ubiquitination. Nature **483:**618-622.

48. **Huang OW, Ma X, Yin J, Flinders J, Maurer T, Kayagaki N, Phung Q, Bosanac I, Arnott D, Dixit VM, Hymowitz SG, Starovasnik MA, Cochran AG.** 2012. Phosphorylation-dependent activity of the deubiquitinase DUBA. Nat Struct Mol Biol **19:**171-175.
49. **Sun Z, Li Y, Ransburgh R, Snijder EJ, Fang Y.** 2012. Nonstructural protein 2 of porcine reproductive and respiratory syndrome virus inhibits the antiviral function of interferon-stimulated gene 15. J Virol **86:**3839–3850.
50. **Durfee LA, Lyon N, Seo K, Huibregtse JM.** 2010. The ISG15 conjugation system broadly targets newly synthesized proteins: implications for the antiviral function of ISG15. Mol Cell **38:**722-732.
51. **Dikic I, Wakatsuki S, Walters KJ.** 2009. Ubiquitin-binding domains - from structures to functions. Nat Rev Mol Cell Biol **10:**659-671.
52. **Gack MU, Shin YC, Joo CH, Urano T, Liang C, Sun L, Takeuchi O, Akira S, Chen Z, Inoue S, Jung JU.** 2007. TRIM25 RING-finger E3 ubiquitin ligase is essential for RIG-I-mediated antiviral activity. Nature **446:**916-920.
53. **Morrison JM, Racaniello VR.** 2009. Proteinase 2Apro is essential for enterovirus replication in type I interferon-treated cells. J Virol **83:**4412-4422.
54. **Ventoso I, Carrasco L.** 1995. A poliovirus 2A(pro) mutant unable to cleave 3CD shows inefficient viral protein synthesis and transactivation defects. J Virol **69:**6280-6288.
55. **Yu SF, Lloyd RE.** 1991. Identification of essential amino acid residues in the functional activity of poliovirus 2A protease. Virology **182:**615-625.
56. **Yu SF, Benton P, Bovee M, Sessions J, Lloyd RE.** 1995. Defective RNA replication by poliovirus mutants deficient in 2A protease cleavage activity. J Virol **69:**247-252.
57. **Kamphuis IG, Kalk KH, Swarte MBA, Drenth J.** 1984. Structure of papain refined at 1.65 ≈ resolution. Journal of Molecular Biology **179:**233-256.
58. **Bergeron E, Albarino CG, Khristova ML, Nichol ST.** 2010. Crimean-Congo hemorrhagic fever virus-encoded ovarian tumor protease activity is dispensable for virus RNA polymerase function. J Virol **84:**216-226.
59. **Bosanac I, Wertz IE, Pan B, Yu C, Kusam S, Lam C, Phu L, Phung Q, Maurer B, Arnott D, Kirkpatrick DS, Dixit VM, Hymowitz SG.** 2010. Ubiquitin Binding to A20 ZnF4 Is Required for Modulation of NF-κB Signaling. Molecular Cell **40:**548-557.
60. **Zhang J, Timoney PJ, Shuck KM, Seoul G, Go YY, Lu Z, Powell DG, Meade BJ, Balasuriya UB.** 2010. Molecular epidemiology and genetic characterization of equine arteritis virus isolates associated with the 2006-2007 multi-state disease occurrence in the USA. J Gen Virol **91:**2286-2301.
61. **Holyoak GR, Balasuriya UB, Broaddus CC, Timoney PJ.** 2008. Equine viral arteritis: current status and prevention. Theriogenology **70:**403-414.
62. **Holtkamp DJ, Kliebenstein JB, Neumann EJ, Zimmerman JJ, Rotto H, Yoder TK, Wang A, Yeske P, Mowrer C, Haley C.** 2011, p 86. International PRRS Symposium, Chicago, Illinois.
63. **Tong GZ, Zhou YJ, Hao XF, Tian ZJ, An TQ, Qiu HJ.** 2007. Highly pathogenic porcine reproductive and respiratory syndrome, China. Emerg Infect Dis **13:**1434-1436.
64. **Li Y, Wang X, Bo K, Tang B, Yang B, Jiang W, Jiang P.** 2007. Emergence of a highly pathogenic porcine reproductive and respiratory syndrome virus in the Mid-Eastern region of China. Vet J **174:**577-584.
65. **Tian K, Yu X, Zhao T, Feng Y, Cao Z, Wang C, Hu Y, Chen X, Hu D, Tian X, Liu D, Zhang S, Deng X, Ding Y, Yang L, Zhang Y, Xiao H, Qiao M, Wang B, Hou L, Wang X, Yang X, Kang L, Sun M, Jin P, Wang S, Kitamura Y, Yan J, Gao GF.** 2007. Emergence of fatal PRRSV variants:

unparalleled outbreaks of atypical PRRS in China and molecular dissection of the unique hallmark. PLoS One **2:**e526.

66. **Kimman TG, Cornelissen LA, Moormann RJ, Rebel JM, Stockhofe-Zurwieden N.** 2009. Challenges for porcine reproductive and respiratory syndrome virus (PRRSV) vaccinology. Vaccine **27:**3704-3718.
67. **Chen Z, Lawson S, Sun Z, Zhou X, Guan X, Christopher-Hennings J, Nelson EA, Fang Y.** 2010. Identification of two auto-cleavage products of nonstructural protein 1 (nsp1) in porcine reproductive and respiratory syndrome virus infected cells: nsp1 function as interferon antagonist. Virology **398:**87-97.
68. **Beura LK, Sarkar SN, Kwon B, Subramaniam S, Jones C, Pattnaik AK, Osorio FA.** 2010. Porcine reproductive and respiratory syndrome virus nonstructural protein 1beta modulates host innate immune response by antagonizing IRF3 activation. J Virol **84:**1574-1584.
69. **Richt JA, Garcia-Sastre A.** 2009. Attenuated influenza virus vaccines with modified NS1 proteins. Current topics in microbiology and immunology **333:**177-195.
70. **Perlman S, Netland J.** 2009. Coronaviruses post-SARS: update on replication and pathogenesis. Nat Rev Microbiol **7:**439-450.
71. **Zaki AM, van Boheemen S, Bestebroer TM, Osterhaus AD, Fouchier RA.** 2012. Isolation of a novel coronavirus from a man with pneumonia in Saudi Arabia. The New England journal of medicine **367:**1814-1820.
72. **van Boheemen S, de Graaf M, Lauber C, Bestebroer TM, Raj VS, Zaki AM, Osterhaus AD, Haagmans BL, Gorbalenya AE, Snijder EJ, Fouchier RA.** 2012. Genomic characterization of a newly discovered coronavirus associated with acute respiratory distress syndrome in humans. mBio 3:e00473-12.
73. **Clementz MA, Chen Z, Banach BS, Wang Y, Sun L, Ratia K, Baez-Santos YM, Wang J, Takayama J, Ghosh AK, Li K, Mesecar AD, Baker SC.** 2010. Deubiquitinating and interferon antagonism activities of coronavirus papain-like proteases. J Virol **84:**4619-4629.
74. **Wojdyla JA, Manolaridis I, van Kasteren PB, Kikkert M, Snijder EJ, Gorbalenya AE, Tucker PA.** 2010. Papain-like protease 1 from transmissible gastroenteritis virus: crystal structure and enzymatic activity toward viral and cellular substrates. J Virol **84:**10063-10073.
75. **Ratia K, Saikatendu KS, Santarsiero BD, Barretto N, Baker SC, Stevens RC, Mesecar AD.** 2006. Severe acute respiratory syndrome coronavirus papain-like protease: structure of a viral deubiquitinating enzyme. Proc Natl Acad Sci U S A **103:**5717-5722.
76. **Fitzgerald KA, McWhirter SM, Faia KL, Rowe DC, Latz E, Golenbock DT, Coyle AJ, Liao SM, Maniatis T.** 2003. IKKepsilon and TBK1 are essential components of the IRF3 signalling pathway. Nat Immunol **4:**491-496.
77. **Gack MU, Albrecht RA, Urano T, Inn KS, Huang IC, Carnero E, Farzan M, Inoue S, Jung JU, Garcia-Sastre A.** 2009. Influenza A virus NS1 targets the ubiquitin ligase TRIM25 to evade recognition by the host viral RNA sensor RIG-I. Cell Host Microbe **5:**439-449.
78. **Versteeg GA, Hale BG, van Boheemen S, Wolff T, Lenschow DJ, Garcia-Sastre A.** 2010. Species-specific antagonism of host ISGylation by the influenza B virus NS1 protein. J Virol **84:**5423-5430.
79. **MacLachlan NJ, Balasuriya UB, Hedges JF, Schweidler TM, McCollum WH, Timoney PJ, Hullinger PJ, Patton JF.** 1998. Serologic response of horses to the structural proteins of equine arteritis virus. Journal of veterinary diagnostic investigation : official publication of the American Association of Veterinary Laboratory Diagnosticians, Inc **10:**229-236.

80. **Malakhov MP, Kim KI, Malakhova OA, Jacobs BS, Borden EC, Zhang DE.** 2003. High-throughput immunoblotting. Ubiquitin-like protein ISG15 modifies key regulators of signal transduction. J Biol Chem **278:**16608-16613.
81. **Gohara DW, Ha CS, Kumar S, Ghosh B, Arnold JJ, Wisniewski TJ, Cameron CE.** 1999. Production of "authentic" poliovirus RNA-dependent RNA polymerase (3D(pol)) by ubiquitin-protease-mediated cleavage in Escherichia coli. Protein Expr Purif **17:**128-138.
82. **Collaborative Computational Project Number 4.** 1994. The CCP4 Suite: Programs for Protein Crystallography. Acta Crystallogr D **50:**760-763.
83. **Adams PD, Afonine PV, Bunkoczi G, Chen VB, Davis IW, Echols N, Headd JJ, Hung L-W, Kapral GJ, Grosse-Kunstleve RW, McCoy AJ, Moriarty NW, Oeffner R, Read RJ, Richardson DC, Richardson JS, Terwilliger TC, Zwart PH.** 2010. PHENIX: a comprehensive Python-based system for macromolecular structure solution. Acta Crystallographica Section D **66:**213-221.
84. **Brunger AT.** 1992. Free R-Value - a Novel Statistical Quantity for Assessing the Accuracy of Crystal-Structures. Nature **355:**472-475.
85. **Emsley P, Cowtan K.** 2004. Coot: model-building tools for molecular graphics. Acta Crystallogr D Biol Crystallogr **60:**2126-2132.
86. **van Dinten LC, den Boon JA, Wassenaar AL, Spaan WJ, Snijder EJ.** 1997. An infectious arterivirus cDNA clone: identification of a replicase point mutation that abolishes discontinuous mRNA transcription. Proc Natl Acad Sci U S A **94:**991-996.
87. **Nedialkova DD, Gorbalenya AE, Snijder EJ.** 2010. Arterivirus Nsp1 modulates the accumulation of minus-strand templates to control the relative abundance of viral mRNAs. PLoS Pathog **6:**e1000772.
88. **Rozen S, Skaletsky HJ.** 1998. Primer3 on the WWW for general users and for biologist programmers, p. pp 365-386. *In* S. K, Misener S (ed.), Bioinformatics Methods and Protocols: Methods in Molecular Biology. Humana Press, Totowa, NJ.
89. **DeLano WL.** 2002. The PyMOL Molecular Graphics System. DeLano Scientific, Palo Alto, CA, USA.

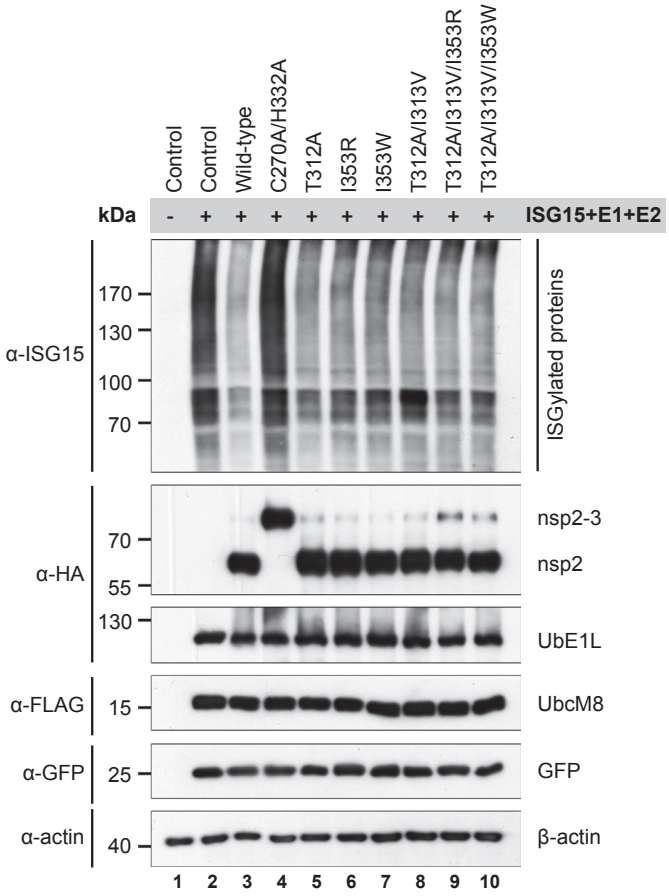

Figure IV-S1. The deISGylating activity of PLP2 is only mildly affected by Ub-binding surface mutations. HEK293T cells were transfected with a combination of plasmids encoding nsp2-3 containing WT or mutant PLP2, GFP, hISG15, and the E1 and E2 enzymes needed for its conjugation: HA-UbE1L and FLAG-UbcM8. ISGylation is visualized on Western blot using an anti-ISG15 antibody.

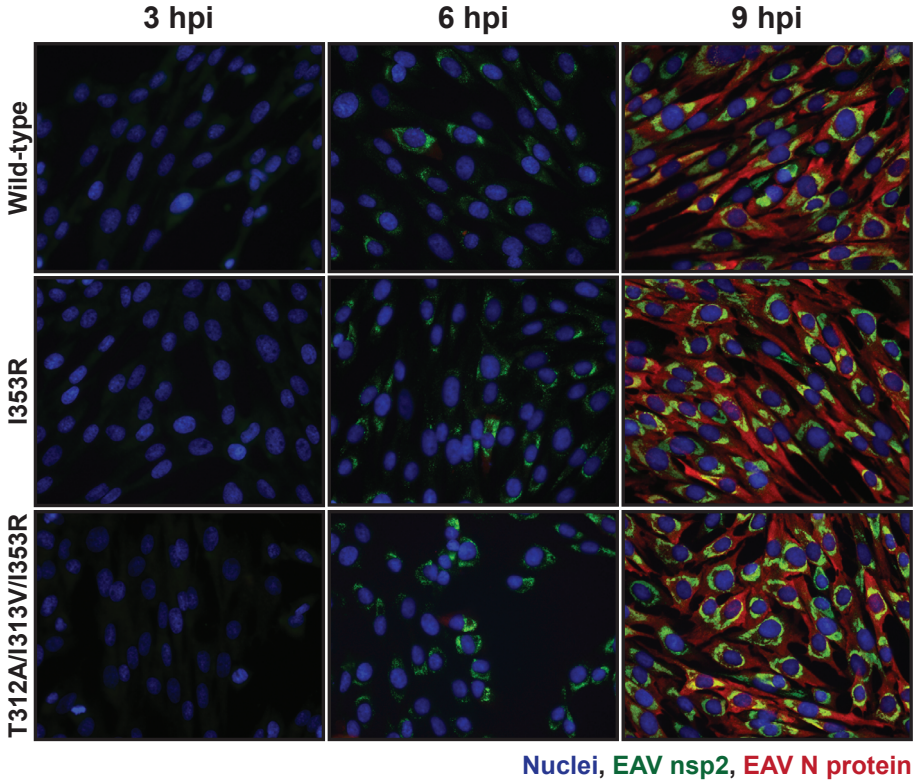

Figure IV-S2. Immunofluorescence microscopy reveals similar replication kinetics for WT and PLP2 mutant viruses. ELFs were infected with WT or mutant EAV at MOI 5. At 3, 6, and 9 hpi, cells were fixed for immunofluorescence microscopy, and EAV nsp2 (green), N protein (red), and nuclei (blue) were visualized using the appropriate antibodies or Hoechst dye, respectively. **Abbreviation:** N, nucleocapsid.

Table IV-S1: Crystallographic data and model refinement statistics.

Crystal geometry			
Space group		$P2_1\,2_1\,2_1$	
Unit cell (Å)		a = 38.32, b = 62.23, c = 84.28 α = β = γ = 90°	
Crystallographic data			
Dataset	Edge (Zinc)	Peak (Zinc)	Remote (Zinc)
Wavelength (Å)	1.28289	1.28243	1.27347
Resolution range (Å)	31.10-1.45 (1.53-1.45)*	31.11-1.45 (1.53-1.45)	31.02-1.45 (1.53-1.45)
Total observations	316923 (34142)	317730 (34806)	317984 (36992)
Unique reflections	36316 (5023)	36344 (5029)	36278 (5075)
Multiplicity	8.7 (6.8)	8.7 (6.9)	8.8 (7.3)
Completeness (%)	99.4 (95.9)	99.4 (96.2)	99.6 (97.1)
Anomalous completeness	99.1 (94.0)	99.2 (94.4)	99.4 (95.8)
R_{merge}	0.054 (0.253)	0.049 (0.205)	0.079 (0.596)
$I/\sigma I$	19.5 (6.0)	21.3 (7.1)	14.7 (4.2)
Phasing statistics			
FOM		0.61	
FOM after RESOLVE		0.72	
Refinement Statistics			
Reflections in test set		1994	
Protein atoms		3155	
Zinc atoms		1	
Solvent atoms		376	
R_{work} (R_{free})		0.16 (0.18)	
Mean B value (Å^2)		19.90	
RMSD from ideal geometry:			
Bond lengths (Å)/angles (°)		0.013/1.47	
Ramachandran plot:			
Most favored/allowed (%)		98/2	

* Values in parentheses refer to the highest resolution shell.

Table IV-S2: Primers used for quantitative real-time PCR.

Target (Accession)	Forward primer (5'-3')	Reverse primer (5'-3')
Equine GAPDH (NM_001163856)	TGCCGCCTGGAGAAAGCTGC	GAGGGCAATGCCAGCCCCAG
Equine Actin-β (NM_001081838)	CCACGCCATCCTGCGTCTGG	ACCGCTCGTTGCCGATGGTG
Equine IFN-β (NM_001099440)	AGGTGGATCCTCCCAATGGCCC	GGGGCAACGTTGAGGGGCTC
Equine MX1 (NM_001082492)	CGGCCAGCAGCTGCAGAAGT	GGCCTCCGCTCCCTGGAGAT
Equine IL8 (NM_001083951)	GCCGTCTTCCTGCTTTCTG	CCGAAGCTCTGCAGTAATTCTTGAT
EAV genome (NC_002532)	CCGACCCGGTGTGACCGTTG	AAGGGTCGCGGGTGCCAATG